Icosahedral alloys grown in Al excess: Problems of disorder and stability

1994 J. Phys.: Condens. Matter 6 2307

(http://iopscience.iop.org/0953-8984/6/12/004)

J. Phys.: Condens. Matter 6 (1994) 2307–2320. Printed in the UK

Icosahedral alloys grown in Al excess: problems of disorder and stability

R Manaila†, A Jianu†, R Popescu‡ and A Devenyi†

† Institute of Physics and Technology of Materials, PO Box MG 7, Bucharest-Magurele, Hungary

‡ Institute of Physical Chemistry, Spl. Independentei 202, 77208 Bucharest, Hungary

Received 3 June 1993, in final form 12 November 1993

Abstract. Phonon- and random-phason-type structural disorder was measured in Al–transition metal (TM) ternary alloys, prepared with Al excess by rapid quenching. The disorder parameters correlate with the calculations on the energy stability of $Al_{12}TM$ icosahedra. Thus, substitution of 'unstable' elements (Fe and Co) for 'stable' elements (Cr and Mn) causes a strong increase in both types of disorder, leading finally to crystallization. This chemical trend is modulated around special compositions of the TM sublattice. The degree of structural order correlates with the thermal stability of icosahedral phases.

1. Introduction

Preparation of icosahedral $Al_{1-y}TM_y$ (i-$Al_{1-y}TM_y$) (TM≡transition metal) alloys in an excess of Al (above the approximate $Al_{80}TM_{20}$ stoichiometry) is frequently used in order to avoid formation of the decagonal phase and to obtain icosahedral phases (i-phases) with well developed morphology. Two widespread methods of preparation have this feature in common;

(1) thin films obtained by sequential vapour deposition of Al and TM layers [1];

(2) melt-quenched ribbons with over-stoichiometric Al content ($y < 0.2$; usually $y \simeq 0.14$) [2, 3].

In both processes, TM atoms are deposited on the surface of (or embedded in) a large Al 'reservoir', in the form of a substrate film or of a matrix. Therefore, the local composition is close to $Al_{12}TM$ ($y \simeq 0.08$), which is known to crystallize (for TM≡Mn, Mo, Tc or W) as $Al_{12}TM$ centred icosahedra, arranged in a BCC lattice.

Carlsson [4, 5] has recently evaluated the relative energy stabilization ΔE of $Al_{12}TM$ lattices of icosahedra, for different TMs belonging to the 3d and 4d periods. For both periods, the stabilization by electronic terms is maximal for half-filled d bands: $\Delta E_{Cr} < \Delta E_{Mn} < \Delta E_{Fe} < 0$; $\Delta E_{Co} > 0$. This energy stabilization (relative to the cubic structures of the Cu_3Au type) mainly relies on a strong non-bonding d-states peak, close to the Fermi level. It is shown [4] to be due to s–d hybridization of the TM orbitals, which is favoured by two structural factors:

(1) a large unit-cell size (inducing closely spaced free-electron states around the bare d-state energy);

(2) no 90° bonding angles of ligands around the TM atoms, a condition fulfilled by the icosahedral local structure.

0953-8984/94/122307+14$19.50

The energy stabilization of $Al_{12}TM$ icosahedral clusters can also be considered as relevant to the formation of extended i-phases. An arrangement of 12 clusters (such that the TM atoms themselves form an icosahedron) is an approximate description for a three-shell Mackay icosahedron [6, 7]. This model is supported by the number of Al neighbours around a TM atom (about 10), as derived from EXAFS data [8]. In crystalline α-Al–Mn–Si, composed of Mackay icosahedra, this coordination is still closer to icosahedral i.e. 11 and 12 for two inequivalent Mn sites [9].

Thus, preparations in Al excess offer a good opportunity to test the predictions on the chemical trends of icosahedral stability, in the simplest case of $Al_{12}TM$ icosahedra. Little attention has been paid until now to the relation between the i-phase stability and icosahedral order, on the one hand, and the composition of the TM sublattice, on the other hand. The present work is concerned with the degree of structural order in i-phases, grown in Al excess in the systems $Al_{86}Cr_{14-x}(Mn, Fe, Co)_x$ and $Al_{86}Mn_{14-x}Fe_x$. It can be assumed that the phonon and phason components of disorder are indicative of the instability of the i-phase towards crystallization. This assumption is supported by the observation that increasing phason disorder causes the i-phases to transform into crystalline phases [10].

Two main types of disorder are usually considered in i-phases: phonon and phason strain. They include distortions in the physical and the complementary spaces; coupled with the reciprocal vectors $G_{\parallel}$ and $G_{\perp}$, respectively, Random-phason disorder is most easily described as fluctuations in the slope of the projection window, within the 'cut-and-project' formalism [11]. Thereby, the slope can approach rational values, characteristic of large-cell approximant lattices, favouring crystallization as a phase transition. An equilibrium concentration of phasons can stabilize certain i-phases at high temperatures, by an entropy mechanism. 'Phonon' disorder comprises random displacive fluctuations of the atomic positions around the equilibrium positions, analogous to the 'static phonons' used in describing glassy structures. It is equivalent to a random inhomogeneous strain affecting the atomic network.

2. Sample preparation

Melt-spun ribbons were prepared with nominal compositions $Al_{86}Cr_{14-x}(Mn, Fe, Co)_x$ (x = 0, 2.8, 5.6, 7, 8.4, 11.2 and 14) and $Al_{86}Mn_{10-x}Fe_x$ (x = 0, 1, 2, 4, 6 and 10). The total TM concentration is thus maintained at 14 at.%, while gradual substitutions are performed between the two TMs. The starting elements were alloyed in the graphite crucible of an induction oven. Pieces of these alloys were melted and pushed through a circular opening (diameter, 0.8 mm) of a quartz crucible by Ar overpressure, against a copper wheel rotating at 2125 rev min^{-1}. The rapidly solidified alloys are obtained as ribbons 0.8–1.2 mm wide and 30–50 μm thick.

3. Experimental details

Phonon- and phason-type disorder in i-phases was evaluated on the basis of x-ray diffraction linewidths. Line profiles were measured on a θ–2θ diffractometer in step-scanning regime ($\Delta(2\theta) = 0.01°$). Cu Kα radiation was used, monochromated by a flat graphite crystal, placed before the scintillation counter. This geometry eliminates most of the fluorescent background contributed by the transition metals. The FWHMs and integral widths were determined after subtracting the background by linear interpolation between the far wings of

the lines. Thereby, the linewidth data are insensitive to any residual fluorescence radiation, which could enter the energy window of the monochromator.

The experimental geometry corresponds to a resolution $\Delta G_{\parallel} = 2.8 \times 10^{-3}$ Å^{-1} ($G_{\parallel} = (4\pi \sin\theta)/\lambda$), as determined with an α-quartz single crystal. Measurements were taken in the fixed-time regime. Flow chart records were also used (counter speed, 2° min^{-1}), but only in order to assess the phase composition.

DTA runs were carried out to check the thermal stability of the alloys. Transmission electron microscopy on thinned samples was performed in the dark-field mode, using the (20, 32) spot in the SAED patterns.

4. Results

4.1. Phase composition

The ribbons were found to consist of an i-phase (or crystalline phase) and excess Al. The system of diffraction lines typical for i-phases [12] was clearly identified (figures 1–3) throughout a composition range which depends on the TM. However, the relatively high level of disorder caused a limited number of lines only (the most intense) to be suitable for linewidth evaluation (table 1). No data on the composition of the i-phase are available, partly because of the small grain size. In the case of i-Al–Mn, agreement between our value for the hypercubic parameter Z (see section 6) and data on $Al_{73}Si_6Mn_{21}$ given in the literature [12] points to a composition close to $Al_{79}Mn_{21}$.

Table 1. Icosahedral diffraction lines used in the evaluation of phonon and phason disorder, with reciprocal vectors $G_{\parallel}$ and $G_{\perp}$. The indices of Cahn *et al* [24] are used. The $G_{\parallel}$- and $G_{\perp}$-values correspond to the i-phase in the $Al_{86}Cr_{14}$ alloy.

Diffraction line	$G_{\parallel}$ (Å^{-1})	$G_{\perp} \times 10^2$ (Å^{-1})
(18, 29)	0.454	2.53
(52, 84)	0.772	2.66
(20, 32)	0.477	4.30
(38, 61)	0.659	4.99
(6, 9)	0.255	6.03

Traces of crystalline θ-$Al_{13}Cr_2$ could be identified in the $Al_{86}Cr_{14}$ sample but were absent in the Al–Cr–(Fe, Co, Mn) samples. Substitution of Cr by Fe, Mn or Co, as well as substitution of Mn by Fe (increasing x) induces shifts in the line position of the i-phase, indicative of a variation in the hypercubic lattice parameter.

Beyond a critical x_{lim}-value, formation of the i-phase is suppressed and crystalline Al–TM compounds appear instead, starting with $x = x_{\text{cr}}$. The values of x_{lim}, x_{cr} and the crystalline phases appearing for $x \geqslant x_{\text{cr}}$ are given in table 2. The latter are not composed of icosahedral clusters.

4.2. Phonon and phason disorder

The full widths at half-maximum (FWHMs) and integral widths of the diffraction lines were determined and expressed in the same units as $G_{\parallel}$. Corrections were applied for the $K\alpha$ doublet and instrumental resolution.

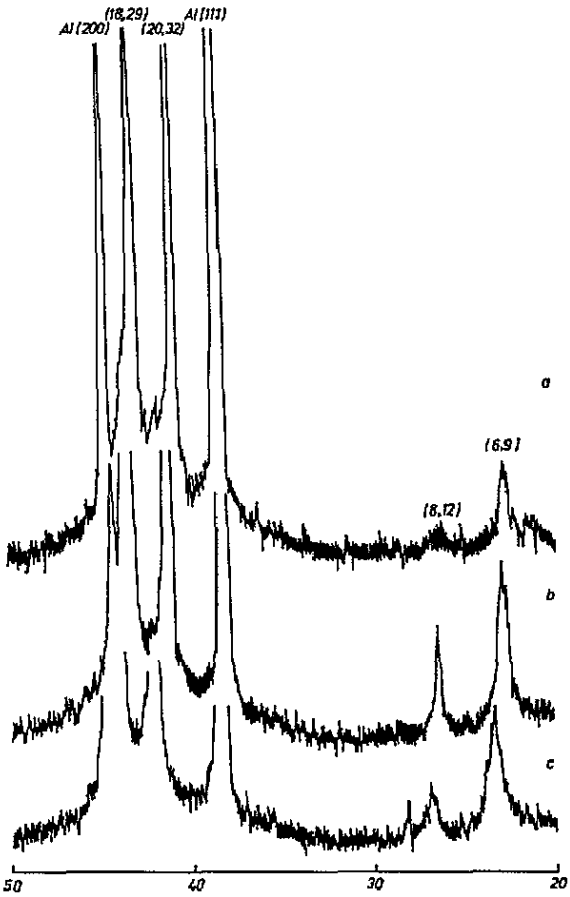

Figure 1. Fragments of XRD patterns, showing the main icosahedral lines in the system Al_{86}–$Cr_{14-x}Fe_x$: curve a, $x = 0$; curve b, $x = 7$; curve c, $x = 11.2$.

The FWHMs show a strong dependence on composition (figure 4), increasing with increasing Fe or Co content for the Cr-based systems (figures 4(a) and 4(b)) or with increasing Fe content for the Mn-based samples (figure 4(c)). The linewidths also show a non-monotonically increasing trend with $G_\perp$, suggesting a mixed dependence on $G_\perp$ and $G_\parallel$. The integral widths follow an evolution with composition and $G_\perp$ which is similar to that found for the FWHMs. The corrected width values B were least squares fitted to the quadratic law

$$B^2 = AG_\parallel^2 + CG_\perp^2 + D \tag{1}$$

which was found to be most suitable in the case of random-phason strain [13, 14]. Here, B stands for the FWHM or the integral width value.

Equation (1) describes the dependence of linewidths on both the parallel and the perpendicular components of the 6D reciprocal vector. The parameters A and C are measures of phonon (static, as well as thermal) and phason disorder, respectively, while the G-independent component D can be attributed to the limited coherence length in the i-phase.

In the fitting process, the linewidth data were weighted by their areas. Calculated FWHM values using best-fit parameters A, C and D are exemplified in figure 4(b). The residual,

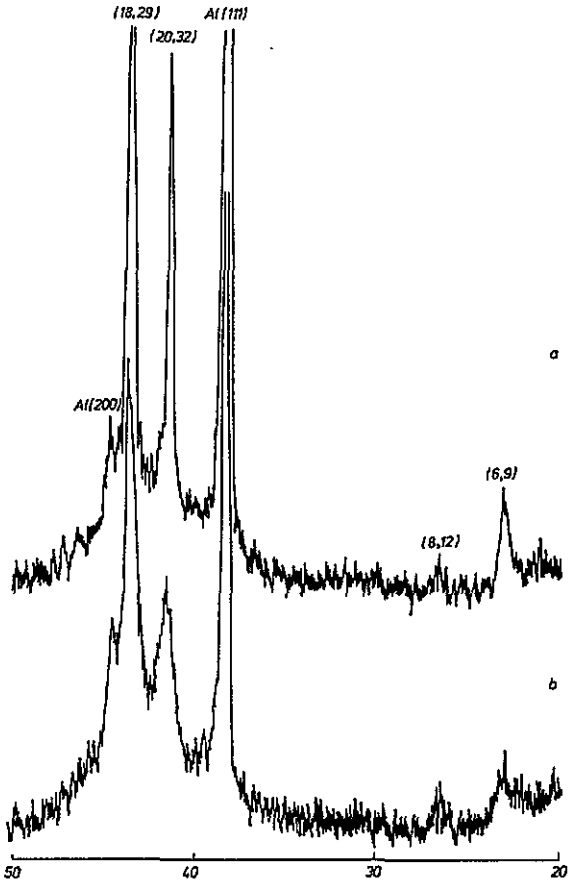

Figure 2. Fragments of XRD patterns, showing the main icosahedral lines in the system Al_{86}–$Cr_{14-x}Co_x$: curve a, $x = 5.6$ curve b, $x = 7$.

defined as

$$R = \sum (B_{\text{calc}} - B_{\text{exp}})^2 \Big/ \sum B_{\text{exp}}^2$$

ranged between 8×10^{-10} and 3×10^{-7}. For samples in the other two systems, values of the FWHM residual were of the same order of magnitude. The A-, C- and D-values thus obtained are plotted in figures 5–7 versus composition. The values of these parameters derived from integral widths were found to follow a similar trend.

4.3. Evolution of phonon and phason disorder with composition

The binary i-phases Al–Cr and Al–Mn have A-values of 1.1×10^{-5} and 1.8×10^{-5} and C-values of 0.47×10^{-2} and 0.68×10^{-2}, respectively. The difference between the parameters of the two compositions lies within the range covered by five Al–Mn preparations (figures 5 and 6). A and C for the Al–Mn i-phase can be compared with the data reported in the literature for Al–Mn evaporated films [13] and melt-spun ribbons [13, 14]. To this effect, the linewidths quoted in [13, 14] were fitted to equation (1). The resulting parameters

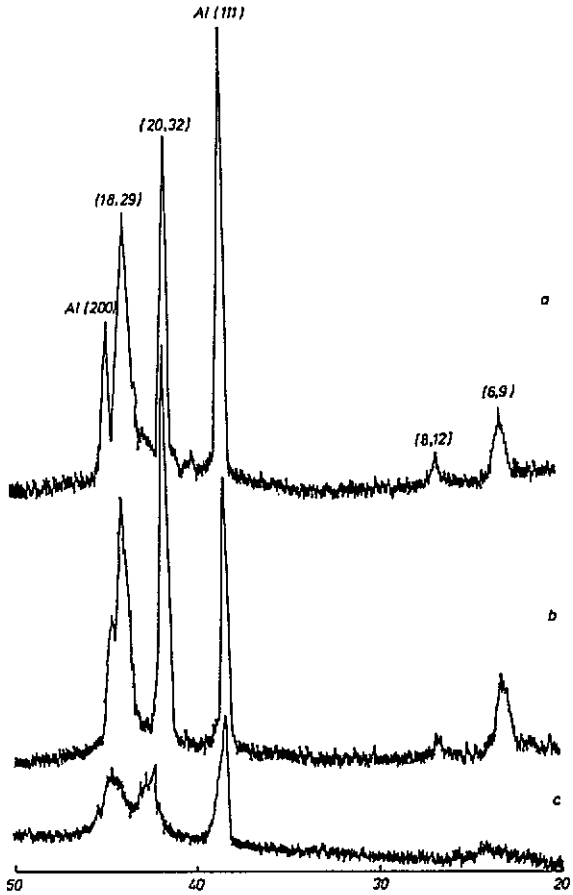

Figure 3. Fragments of XRD patterns, showing the main icosahedral lines in the system $Al_{86}Mn_{14-x}Fe_x$: curve a, $x = 0$; curve b, $x = 4$; curve c, $x = 10$.

Table 2. Upper limit x_{lim} of the i-phase range, lower limit x_{cr} of the crystalline range, compositional zone x_{TCP} of crystalline TCP phases and crystalline phases present for $x \geqslant x_{cr}$.

System	x_{lim}	x_{cr}	x_{TCP}	Crystalline phases
$Al_{86}Cr_{14-x}Mn_x$	[a]	[a]	9.4–10.5	—
$Al_{86}Cr_{14-x}Fe_x$	11.2	14	7.0–7.6	$Al_{13}Fe_4$[d]
$Al_{86}Cr_{14-x}Co_x$	7[b]	8.4	4.9–6.0	Al_9Co_2 type[e]
$Al_{86}Mn_{14-x}Fe_x$	10	14	4.5[c]	$Al_{13}Fe_4$[d]

[a] i-phases only are present in the whole composition range investigated.
[b] Possibly a transient i-phase; see section 4.3.
[c] Solubility limit of Fe in crystalline α-Mn.
[d] monoclinic $C2/m$.
[e] Monoclinic $P21/a$.

$A = (1\text{–}3) \times 10^{-5}$ Å^{-1} are within our range, while C-values (about 1×10^{-3}) are definitely lower than in our samples. The disorder parameters measured by Calvayrac *et al* [12] on rapidly quenched $Al_{73}Mn_{21}Si_6$ alloys are $A \simeq 2.5 \times 10^{-5}$ Å^{-1} and $C \simeq 1.4 \times 10^{-3}$ Å^{-1}, in

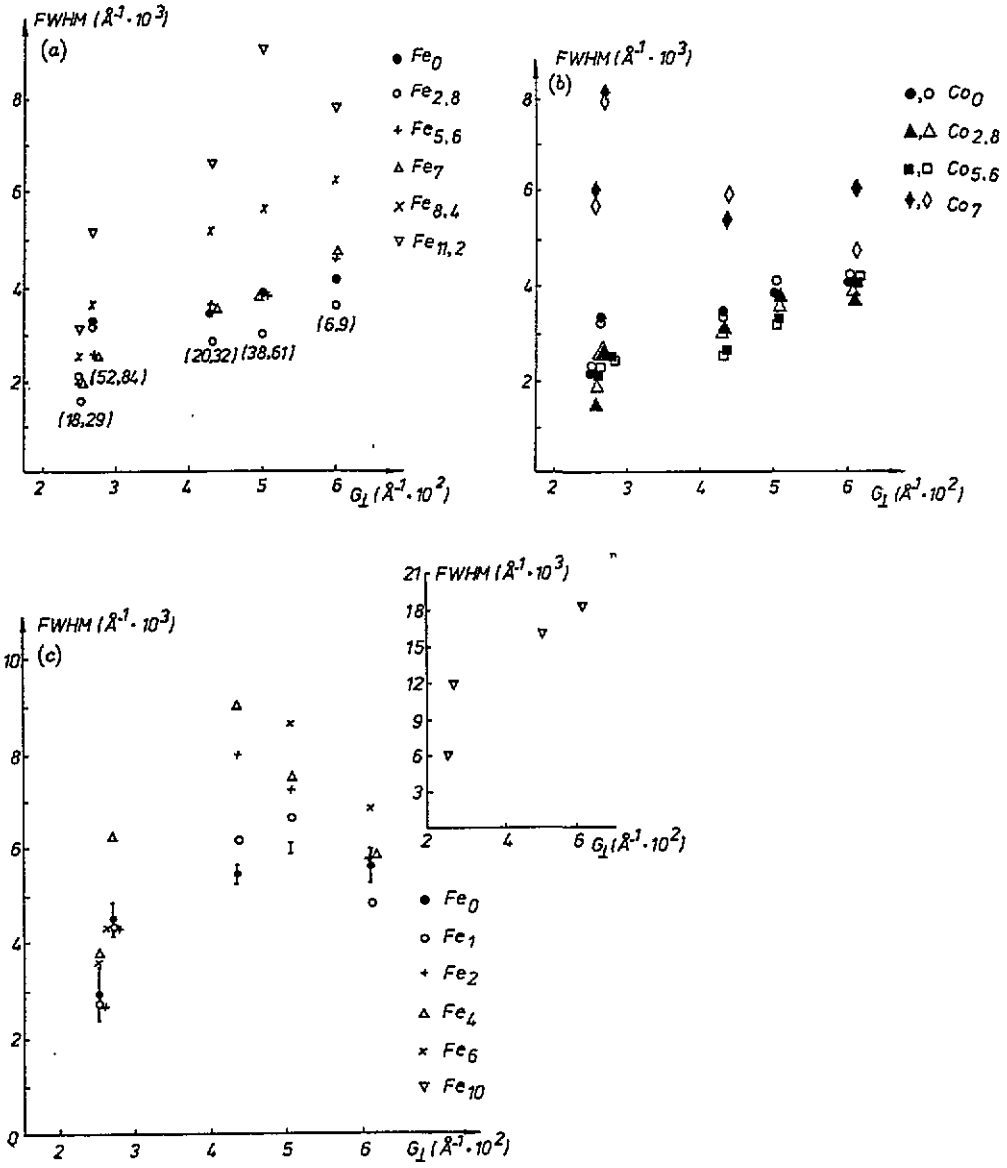

Figure 4. Experimental corrected FWHMs versus $G_\perp$ for icosahedral lines in the following systems: (*a*) Al–Cr–Fe; (*b*) Al–Cr–Co (full symbols, experimental; open symbols, calculated with best-fit parameters); (*c*) Al–Mn–Fe (the inset shows the Fe_{10} sample). The FWHMs are expressed in $G_\parallel$ units.

good agreement with the values derived from the experimental FWHMs reported in [13, 14].

The evolution of the disorder parameters A and C with composition in Cr- and Mn-based systems deserves a closer look.

The substitution of Fe and Co (icosahedrally 'unstable') for Cr and Mn (more 'stable' in the sense of Carlsson [4]) is seen (figures 5 and 6) to cause a general increase in the phonon and phason disorder of the i-phase, beyond some critical system-dependent composition.

The highly disordered composition at $x = x_{\text{lim}}$, beyond which the i-phase alloy

crystallizes (see figures 1(*c*), 2(*b*) and 3(*c*)) could be in principle suspected of being a crystalline approximant of the i-phase. As shown by Calvayrac and Quivy [15] for the case of the i-$Al_{65}Cu_{20}Fe_{15}$ phase, formation of the 3/2 rhomohedral approximant causes a splitting of the icosahedral lines into several peaks, subtending a $\delta G_{\parallel}$-range which increases with increasing $G_{\perp}$. For the maximal $G_{\perp}$ which could be reached in our alloys (limited by disorder and low intensity), this splitting is estimated (after [15]) as $\delta G_{\parallel} \simeq 1.1 \times 10^{-2}$ Å^{-1}, i.e. higher than the high-$G_{\perp}$ experimental FWHMs (figure 4). Therefore, we have to attribute the large linewidths (especially close to x_{lim}) to intrinsic disorder of the i-phase. This conclusion is supported by the fact that the rhomohedral splitting $\delta G_{\parallel}$ is not dependent on $G_{\parallel}$ [15]. Therefore, crystallization in an approximant would cause an increased C but a lower A. On the contrary, in our alloys the high C-value close to x_{lim} (figure 6) is accompanied by a high A-value (figure 5). This observation supports the assumption of intrinsic icosahedral disorder induced by Fe and Co in Cr-based and Mn-based systems. This disorder is to be attributed to both phason and phonon strain.

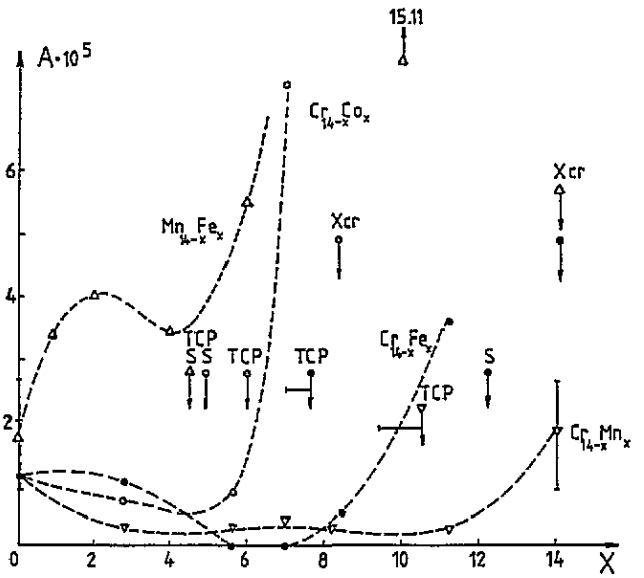

Figure 5. Phonon disorder parameter A versus composition: ●, Al–Cr–Fe; ○, Al–Cr–Co; △, Al–Mn–Fe; ▽, Al–Cr–Mn; S, high-temperature solubilities in crystalline TM1–TM2 systems; TCP, range of TCP crystalline TM1–TM2 alloys; x_{cr}, x at which crystallization occurs; I, range of five Al–Mn preparations.

The distortions induced by Fe and Co in the i-phase increase with increasing x in a non-monotonic way (figures 5 and 6). The composition of the TM subnetwork $(Cr, Mn)_{14-x}(Fe, Co)_x$ seems to play here a special role. Up to a certain x, which depends on the system investigated, the Fe or Co substitution has little effect, the A- and C-values being almost constant (for Al–Cr–Fe and Al–Cr–Co), or increasing slightly (for Al–Mn–Fe). In this range, the parameter D (figure 7) shows a steep increase, suggesting that the disordering effect is 'absorbed' into a decrease in the coherence length (block fragmentation).

Beyond the critical x-value, the phonon and phason disorder shows an abrupt increase (figures 5 and 6), while the icosahedral character of the phase is still preserved (figures 1–3)

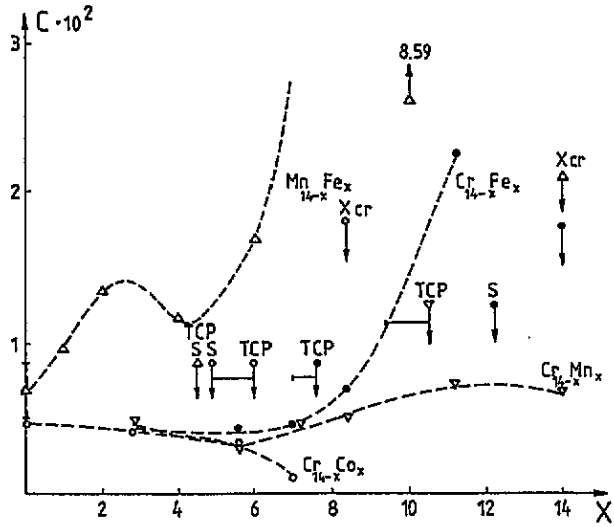

Figure 6. Random phason disorder parameter C versus composition: ●, Al–Cr–Fe; ○, Al–Cr–Co; △, Al–Mn–Fe; ▽, Al–Cr–Mn; S, high-temperature solubilities in crystalline TM1–TM2 systems; TCP, range of TCP crystalline TM1–TM2 alloys; x_{cr}, x at which crystallization occurs; I, range of five Al–Mn preparations.

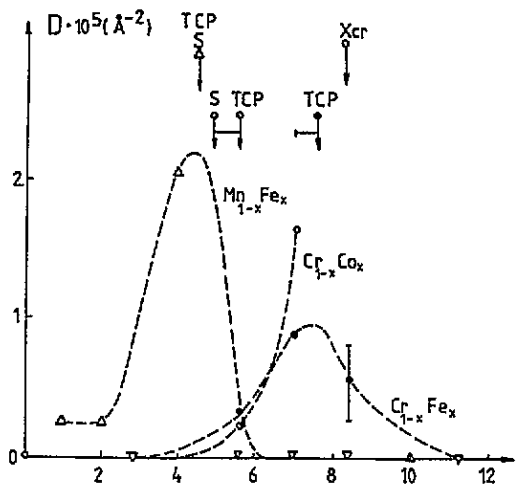

Figure 7. Inverse of coherence length versus composition: ●, Al–Cr–Fe; ○, Al–Cr–Co; △, Al–Mn–Fe; ▽, Al–Cr–Mn; S, high-temperature solubilities in crystalline TM1–TM2 systems; TCP, range of TCP crystalline TM1–TM2 alloys; x_{cr}, x at which crystallization occurs.

(see also comment above). In this range, the D-values decrease (figure 7) corresponding to a very small contribution of limited coherence length to the linewidth.

The Co-richest i-phase in the Al–Cr–Co series ($x = x_{lim} = 7$) is an exception to this general behaviour. The C-value is seen to decrease (figure 6), corresponding to a weaker dependence on $G_\perp$, while A suggests high phonon distortions (figure 5). This structure is possibly transitional towards the Al_9Co_2-type crystalline phase, which was found in samples

with $x > 7$.

The $Al_{86}Cr_{14-x}Mn_x$ system shows only i-phases throughout the whole compositional range ($0 \leqslant x \leqslant 14$). The disorder parameters A and C are low (figures 5 and 6), while the coherence length contribution D (figure 7) is negligible.

5. Role of the transition-metal subnetwork

We tried to correlate the critical x-value in each system with particular compositions in the equilibrium phase diagram of relevant crystalline TM1–TM2 alloys. The critical x-value, up to which i-phases are formed, cannot be clearly associated with the solubility of Fe and Co in Cr or Mn, even if high-temperature solubility values are considered [16] (figures 5–7). However, the tetrahedrally close-packed (TCP) compositions in figure 5–7 seem to correlate with this critical x. The TCP ranges correspond, in the equilibrium phase diagram of TM1–TM2 metals, to TCP structures. TCP lattices can be viewed as an interconnection of TM polyhedra, each TM atom being highly coordinated (Z =12–16). α-Mn belongs to this structural type, as well as σ- and β-U-type phases [17]. However, in TMs and their alloys, stable TCP structures are generally found in limited compositional ranges. Some examples thereof are [17] α-$Mn_{1-y}Fe_y$ for y below the solubility limit (about $\simeq 0.32$), σ-$Cr_{1-x}Fe_x$ ($x = 0.50$–0.54), $Cr_{1-x}Co_x$ ($x = 0.35$–0.43) and $Cr_{1-x}Mn_x$ ($x = 0.67$–0.75). These TCP phases bear a certain structural similarity to the TM sphere of two-shell (or three-shell) Mackay icosahedra. The common feature is that TM atoms in both structures are highly coordinated.

The data on the composition-induced disorder (figures 5 and 6) suggest that the TM subnetwork of the i-phase is really important for the structural order of the whole. The special TCP compositions in each system (as concerns the TM subnetwork) seem to ensure a better structural ordering of the i-phase, expressed by low values of the disorder parameters A and C. In the Cr–Fe and Mn–Fe system, a shallow minimum of A is even suggested (figure 5) around the TCP composition. Janot *et al* [18] also reported that Al–($Fe_{0.5}Cr_{0.5}$) alloys yield well ordered i-phases, which cannot be obtained at other Fe to Cr ratios.

If icosahedral order and energy stabilization are indeed correlated, the special TCP compositions should also be manifest in the thermal stability data. The DTA curves show exothermal effects around a temperature T_c, which was identified as the crystallization point of the i-phase. Figure 8 shows that compositions around TCP possess a higher thermal stability than the end binary alloys. The presence of a small crystallization effect in the mostly crystallized $Al_{86}Fe_{14}$ alloy points to the presence of some small icosahedral fraction, besides the prevailing crystalline $Al_{13}Fe_4$. As reported by Inoue *et al* [19], two-stage crystallization occurring for certain compositions of i-(Al–Cr) alloys (including a metastable intermediate phase) decreases T_c by about 19 K. However, this effect is definitely too small to account for our compositional variation in T_c across the Cr-based systems. Therefore, the results speak for a chemical trend of the icosahedral network stability.

The onset crystallization temperature found for the $Al_{86}Cr_{14}$ alloy (about 643 K) compares well with that reported in [19] for the i-phase containing 14.5 at.% Cr (644 K).

6. Parameter of the hypercubic lattice

The parameter Z of the hypercubic lattice was determined for i-phases of different compositions, using the equation

$$G_{\parallel} = \frac{2\sin\theta}{\lambda} = \frac{(N + M\tau)^{1/2}}{Z[2(2+\tau)]^{1/2}}$$

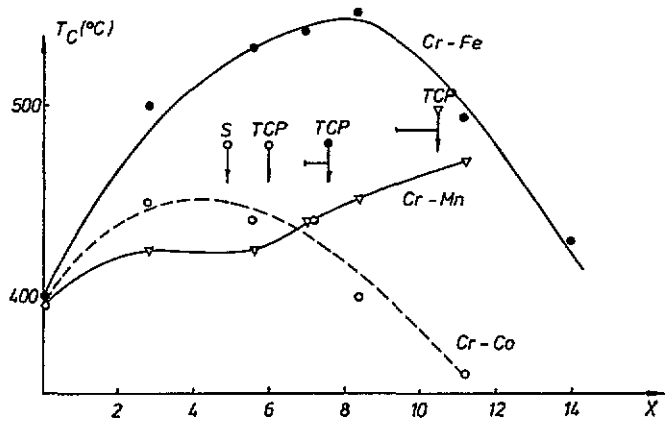

Figure 8. Crystallization temperature T_c of the i-phase in the Al–Cr–(Mn, Fe, Co) systems. The lines are guides to the eye. The values reported correspond to the peak of the exothermal effect.

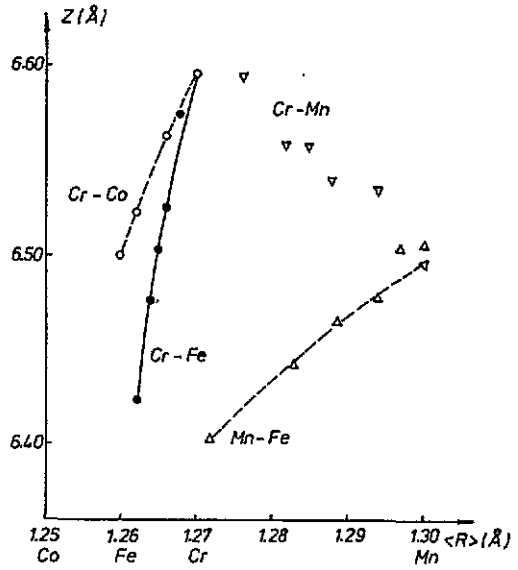

Figure 9. The parameter Z of the hypercubic lattice versus the average TM radius in the system Al–Cr–Fe (●), Al–Cr–Co (○), Al–Mn–Fe (△) and Al–Cr–Mn (▽): ▼, data from [12].

$$G_\perp = \frac{[\tau(N\tau - M)]^{1/2}}{Z[2(2+\tau)]^{1/2}} \qquad \tau = \tfrac{1}{2}\left(1+\sqrt{5}\right).$$

The corrected value (figure 9) for each sample was derived from the Z-values yielded

by different diffraction lines, by at least-squares linear fit $Z(\cos\theta\cot\theta)$, extrapolated to $\theta = 90°$. This procedure eliminates most effects of the diffractometric geometrical aberrations on line positions.

Figure 9 shows that Z increases with increasing average radius of the TM occupying the second shell of the Mackay icosahedron. However, the Cr-based phases follow a trend which is definitely different from that of the Mn-based phases. This suggests that the hypercubic lattices of the two systems are not isomorphous and neither are the Co and Fe substitutions for Cr. The Al–Cr–Mn samples have a Z which varies continuously between the two limiting binary alloys.

On the another hand, the continuous variation in Z with composition within a given system (even for the most distorted samples) confirms their icosahedral nature throughout the compositional range with $x \leqslant x_{\text{lim}}$.

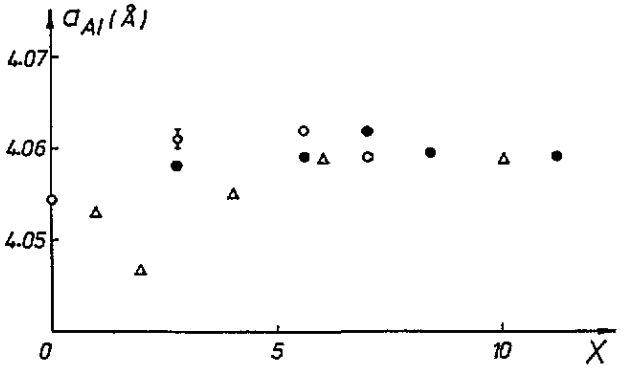

Figure 10. Lattice parameter of the excess Al versus sample composition in the systems $Al_{86}Cr_{14-x}Fe_x$ (●), $Al_{86}Cr_{14-x}Co_x$ (○) and $Al_{86}Mn_{14-x}Fe_x$ (△). The error bar corresponds to the maximal deviation between the two extrapolation methods (see text).

The lattice parameter of the excess Al (figure 10) was derived from the (111), (200), (220) and (311) diffraction lines, by extrapolation to $\theta = 90°$ against a $\cos\theta\cot\theta$ or $\cot^2\theta$ function. It is found to be hardly dependent on the TM composition. Comparing the experimental a_{Al} with the value reported by Mondolfo [20] suggests that the Al matrix dissolves no more than 1.3–1.6% of the TMs. This conclusion was reached on the basis of the a_{Al} quoted [20] for concentrations up to 8 at.% of different TMs (Mn, Fe and Cr) dissolved in Al.

7. Electron microscopy investigations

Dark-field TEM and SAED images were obtained on thinned samples in the $Al_{86}Mn_{14-x}Fe_x$ system ($x = 0$, 2, 4 and 6). Details of the observations have been reported in [21].

SAED patterns revealed the presence of five-fold symmetry axes. Distortions of weak spots characteristic of phason strain were found to increase with increasing x, as well as spot broadening, which can be associated with phonon-type disorder.

In the dark-field images, domains with fringe-like contrast were noticed for $x = 2$–6, with a periodicity of 7–10 nm. These fringes are indicative of limited coherence regions, related to the Fe-induced phason strains.

For the $x = 6$ sample, fragmentation of the dendritic formations occurs, in comparison with lower-Fe-content samples.

8. Comments and conclusions

Rapidly quenched alloys prepared with Al excess in the Al–Cr–(Mn, Fe, Co) and Al–Mn–Fe systems show highly disordered i-phases. They apparently bridge the gap between the nearly 'perfect' i-phases (Al–Cu–Fe and Al–Pd–Mn) and the icosahedral (usually fragmentary) clusters which are often recognized in amorphous (and even in liquid) metals. Amorphous i-phases have already been reported in the Al–Cu–V system [22], a fact which is possibly related to the poor stability of the $Al_{12}V$ icosahedra [4].

Investigating this particular class of icosahedral alloys offers an opportunity to find a relationship between their widely different degrees of order and the energy stabilities of local icosahedral formations of Al_{12}TM.

Gradual substitution of Cr by Fe and Co as well as substitution of Mn by Fe results in an increase in both phonon- and phason-type disorder, finally causing crystallization of the i-phase beyond a critical x_{cr}. For the Co substituent, the crystallization occurs earlier ($x_{cr} = 8.4$) than in the case of Fe substituting for Cr ($x_{cr} = 14$). On the other hand, in the $Al_{86}Cr_{14-x}Mn_x$ system, no crystalline phases are noted. All these observations show that the energy stability of the icosahedral formations decreases in the order $Al_{12}Cr \simeq Al_{12}Mn > Al_{12}Fe > Al_{12}Co$. The result is in agreement with the calculations of stabilization energy reported by Carlsson [4]. However, the disorder increase with increasing concentration of an 'unstable' element was found to be non-monotonic. If a TCP phase is present at some x_{TCP} in the TM1–TM2 crystalline phase diagram, the range $0 < x < x_{TCP}$ shows a relatively low disorder, followed by steep increases in A and C beyond x_{TCP}. Therefore, the experimental evidence suggests that, besides the electronic and geometric factors, the composition of the TM sublattice plays an important topological role in the stability of the i-phase as a whole.

These conclusions on structural disorder show that the most adequate model for the i-phase in Al-excess alloys is a spatial linking of Al_{12}TM icosahedra, whose local stability entails the stability of the whole. This model is close to the concept of 'icosahedral glass' [23].

Acknowledgment

We are indebted to the Alexander von Humboldt Foundation for financial support.

Note added in proof. The average R values in figure 9 were calculated with an Mn radius of 1.30 Å, present in close-packed Mn modifications (metallic valence 4.5). Using instead the value 1.268 Å (metallic valence 6), fully rationalizes the $Z(R)$ dependence, bringing all points close to the same curve (R Manaila *et al*, to be published). This points to a relationship between metallic bond hybridization and local symmetry around Mn atoms.

References

[1] Barna P B, Csanady A, Timmer U and Urban K 1992 *J. Mater. Res.* **7** 1115
[2] Janot Ch, Pannetier J, Dubois J M, Houin J P and Weinland P 1988 *Phil. Mag.* B **58** 59
[3] Manaila R, Florescu V, Jianu A and Radulescu O 1989 *Phil. Mag.* B **60** 589
[4] Carlsson A E 1991 *Phys. Rev.* B **43** 12 176

[5] Carlsson A E 1992 *Phys. Rev.* B **45** 7511
[6] Redfield A C and Zangwill A 1987 *Phys. Rev. Lett.* **58** 2322
[7] Yang Q B 1988 *Phil. Mag.* B **58** 47
[8] Heiney P A, Bancel P A, Goldman A I and Stephens P W 1986 *Phys. Rev.* B **34** 6746
[9] Cooper M and Robinson K 1966 *Acta Crystallogr.* **20** 614
[10] Li F H, Pan G Z, Tao S Z, Hui M J, Mai Z H, Chen X S and Cai L Y 1989 *Phil. Mag.* B **59** 535
[11] Stephens P W 1989 *Aperiodicity and Order* vol 3, ed M V Jaric (New York: Academic) p 37
[12] Calvayrac Y, Quivy A and Gratias D 1989 *Phil. Mag.* B **59** 439
[13] Horn P M, Malzfeldt W, DiVincenzo D P, Toner J and Gambino R 1986 *Phys. Rev. Lett.* **57** 1444
[14] Bancel P A and Heiney P A 1986 *Phys. Rev.* B **33** 7917
[15] Calvayrac Y and Quivy A 1990 *J. Physique* **51** 417
[16] Hansen M and Anderko K 1958 *Constitution of Binary Alloys* (New York: McGraw-Hill)
[17] Shoemaker D P and Shoemaker C B 1988 *Aperiodicity and Order—Introduction to Quasicrystals* vol 1, ed M V Jaric (New York: Academic) p 1
[18] Janot Ch, Pannetier J, Dubois J M and Fruchart R 1986 *Phys. Lett.* **119A** 309
[19] Inoue A, Kimura H and Masumoto T 1987 *J. Mater. Sci.* **22** 1758
[20] Mondolfo L F 1976 *Aluminium Alloys* (London: Butterworths)
[21] Nistor L C, Teodorescu V S and Manaila R 1993 *Microsc. Res. Technol.* **25** 183
[22] Tsai A P, Inoue A, Bizen Y and Masumoto T 1989 *Acta Metall.* **37** 1443
[23] Stephens P W and Goldman A I 1986 *Phys. Rev. Lett.* **56** 1168
[24] Cahn J W, Schechtman D and Gratias G 1986 *J. Mater. Res.* **1** 13